Nuclear Engineering and Technology 53 (2021) 2629–2639

Contents lists available at ScienceDirect

Nuclear Engineering and Technology

journal homepage: www.elsevier.com/locate/net

Original Article

Microstructural characteristics of a fresh U(Mo) monolithic mini-plate: Focus on the Zr coating deposited by PVD

Xavière Iltis [a, *], Doris Drouan [a], Thierry Blay [a], Isabelle Zacharie [a], Catherine Sabathier [a], Claire Onofri [a], Christian Steyer [b], Christian Schwarz [b], Bruno Baumeister [b], Jérôme Allenou [c], Bertrand Stepnik [c], Winfried Petry [b]

[a] CEA, DES, IRESNE, DEC, Cadarache, F-13108, Saint Paul Lez Durance, France
[b] Forschungs-Neutronenquelle Heinz Maier-Leibnitz (FRM II), Technische Universität München, Lichtenbergstr. 1, D-85747, Garching, Germany
[c] FRAMATOME, CERCA, SPL, ZI Les Bérauds, 54 Av. de la Déportation, BP 114, F-26104, Romans sur Isère, France

ARTICLE INFO

Article history:
Received 1 December 2020
Received in revised form
25 February 2021
Accepted 26 February 2021
Available online 3 March 2021

Keywords:
U(Mo)
Monolithic
Coating
Microstructure

ABSTRACT

Within the frame of the EMPIrE test, four monolithic mini-plates were irradiated in the ATR reactor. In two of them, the monolithic U(Mo) foil had been PVD-coated with Zr before the plate manufacturing. Extensive microstructural characterizations were performed on a fresh archive mini-plate, using Optical Microscopy (OM), Scanning Electron Microscopy (SEM) combined with Energy Dispersive Spectroscopy (EDS), Electron Backscattered Diffraction (EBSD) and Focused Ion Beam (FIB)/Transmission Electron Microscopy (TEM) with nano EDS. A particular attention was paid to the examination of the U(Mo) foil, the PVD coating, the cladding/Zr and Zr/U(Mo) interfaces.

The Zr coating has a thickness around 15 μm. It has a columnar microstructure and appears dense. The cohesion of the cladding/Zr and Zr/U(Mo) interfaces seems to be satisfactory. An almost continuous layer with a thickness of the order of 100–300 nm is present at the cladding/Zr interface and corresponds to an oxidized part of the Zr coating. At the Zr/U(Mo) interface, a thin discontinuous layer is observed. It could correspond to locally oxidized U(Mo).

This work provides a basis for interpreting the results of characterizations on EMPIrE irradiated plates.

1. Introduction

Nuclear Materials Testing Reactors (MTRs) require fuel that generates high neutron flux. To obtain sufficient neutronic performance, high enriched uranium (>20% ^{235}U) was used for decades. Most of the time, the fuel elements of MTRs comprised fuel plates in which the fissile material (often UAl_x, i.e. a mixture of uranium aluminides) was in powder form and was dispersed within an aluminium matrix, to form a fuel meat cladded by aluminium alloy plates [1]. To comply with the non-proliferation treaty recommendations, a worldwide effort has been launched since the 1970's to convert MTRs to low enriched uranium (<20% ^{235}U).

The development and qualification of an U_3Si_2-based dispersion fuel [2] allowed converting a significant number of MTRs. However, some high performance reactors could not be converted with this type of fuel, without critical performance losses. This issue led to studies on uranium-molybdenum alloys (U(Mo)), either in a dispersed form or in a monolithic form for most powerful reactors [3].

U(Mo) monolithic fuel consists in a thin (typically about 300 μm thick) uranium-molybdenum alloy (molybdenum content: around 10 wt%) foil, cladded by aluminum alloy sheets. A zirconium barrier layer, which can be added by different methods, is placed between the foil and the cladding, to avoid the formation of a U(Mo)/Al interdiffusion layer which would degrade the fuel performance under irradiation [4]. In the process developed in the United States so far, the U(Mo) foil is first co-rolled with Zr sheets, the Zr-coated foils are then cold-rolled to final thickness and finally bonded to the cladding using Hot Isostatic Pressing (HIP) [5]. Such types of plates were characterized before [6–8] and after irradiation [9,10].

The EMPIrE (European Mini Plate Irradiation Experiment) irradiation experiment performed in the Advanced Test Reactor (ATR), in the United States (US), included four monolithic mini-plates [11]. Two types of monolithic plates were manufactured for this

* Corresponding author.
E-mail address: xaviere.iltis@cea.fr (X. Iltis).

https://doi.org/10.1016/j.net.2021.02.026

irradiation. In both cases, a U + Mo alloy with 10 wt% Mo was melted, cast and rolled by BWXT (US) to obtain an about 330 μm thick foil. This foil was covered by a Zr diffusion barrier either by co-rolling at BWXT, or by a Physical Vapor Deposition (PVD) process, developed at the Technical University of Munich (TUM, Germany) [12]. The Zr coated U(Mo) foil was then cladded with an aluminium alloy (AlFeNi), using the C2TWP process developed by Framatome-CERCA (France) [13].

Zr-PVD coated U(Mo) monolithic fresh fuel has never been subjected to a detailed microstructural examination, to our best knowledge. Performing such an examination, using complementary characterization tools, constitutes the goal of this study. Optical Microscopy (OM) examinations and Scanning Electron Microscopy (SEM) observations coupled with analyses by Energy Dispersive Spectrometry (EDS) were conducted first. Electron BackScattered Diffraction (EBSD) acquisitions were also made in the U(Mo) foil, the Zr coating and the Al cladding. Finally, thin foils were prepared at the U(Mo)/Zr and cladding/Zr interfaces, by Focused Ion Beam (FIB) milling, and examination of these foils were performed by Transmission Electron Microscopy (TEM), Scanning Transmission Electron Microscopy (STEM) and EDS. As C2TWP is a proprietary process, some details about the cladding characteristics are not given.

2. Experimental details

2.1. Sample characteristics and preparation

The size of the EMPIrE mini-plates manufactured by rolling at Framatome-CERCA is 25.4 mm wide, 101.6 mm long and 1.27 mm thick, and the size of the fuel meat zone is 19.1 × 82.6 × 0.51 mm^3, for plates made with dispersion fuel [14]. The piece studied in this paper comes from the n° 1205 archive mini-plate. It was cut by punching and its size was about 9 × 17 mm^2. Four samples were cut from it, using a wire saw: two longitudinal ones, called L1 and L2 (about 9 × 1.7 mm^2) and two transversal ones, called T3 and T4 (about 7 × 1.7 mm^2), as shown in Fig. 1. "Longitudinal" and "transversal" refer to the directions with respect to rolling (see Fig. 1b). The doubling of each type of sample was intended to accelerate the characterization program, as examinations were performed in two different facilities at CEA Cadarache: the UO_2 Laboratory and the LECA-STAR facility.

These four samples were embedded in cross-section, in an Al compact of 12 mm diameter prepared by cold pressing an Al powder, to obtain relatively small metallic samples suitable for SEM and EBSD characterizations and also for FIB milling. They were then mechanically polished. The polished side corresponds to the thickest line delimiting each sample in Fig. 1b. Mechanical polishing for OM and SEM examinations included classical polishing steps with a finish polishing with a colloidal silica suspension. An additional gentler polishing step with a diluted silica suspension was performed just before performing EBSD analyses, as detailed in Ref. [15]: the obtained surface quality was appropriate for acquiring EBSD maps in the U(Mo) foil and in the cladding, but not in the Zr coating. To overcome this limitation, some areas including the Zr layer were prepared by FIB ion etching, using a methodology close to that described in Ref. [15].

2.2. Characterization equipment and methods

Examinations by OM were performed with an Olympus DSX-500 opto-numerical microscope. SEM + EDS analyses were carried out with a FEI Nova NanoSEM450 equipped with an Oxford Instruments EDS detector with an active surface of 20 mm^2, driven by the AZTEC software. A shielded Auriga 40 SEM-FIB from CARL ZEISS was used for the ion-milling of chosen samples. Both SEMs were equipped with a Nordlys II Nano EBSD camera (maximum resolution: 1344 × 1024 pixels) from Oxford Instruments, driven by the AZTEC software. TEM and STEM + EDS examinations were performed with a Thermo Scientific TALOS F200S TEM, equipped with two Thermo Scientific EDS detectors with a 0.45 sr solid angle of collection.

As mentioned previously, some characterizations were performed in the UO_2 Laboratory (devoted to the study of uranium-base fresh fuels) and the other ones were carried out in the LECA-STAR facility (hot laboratory used for studying irradiated fuels), where the SEM-FIB and the TEM are available. The samples used in each case are specified in Table 1.

EBSD analyses were performed with the 1 × 1 or 2 × 2 binning modes of the camera, depending on the quality of the Electron Back Scatter Patterns (EBSPs). EBSPs were indexed using the "refined accuracy" mode in AZTEC that improves the Kikuchi band detection [16]. The three following phases were considered: γ-U(Mo) (body-centered cubic, space group: 229), Zr (hexagonal, space group: 194), Al (face-centered cubic, space group: 225).

Table 1
Characterizations performed on each sample.

Sample	L1	L2	T3	T4
OM	x	x	x	x
SEM		x		x
SEM + EDS	x		x	
EBSD after mechanical polishing	x			
EBSD after FIB milling		x		x
TEM + STEM + EDS				x

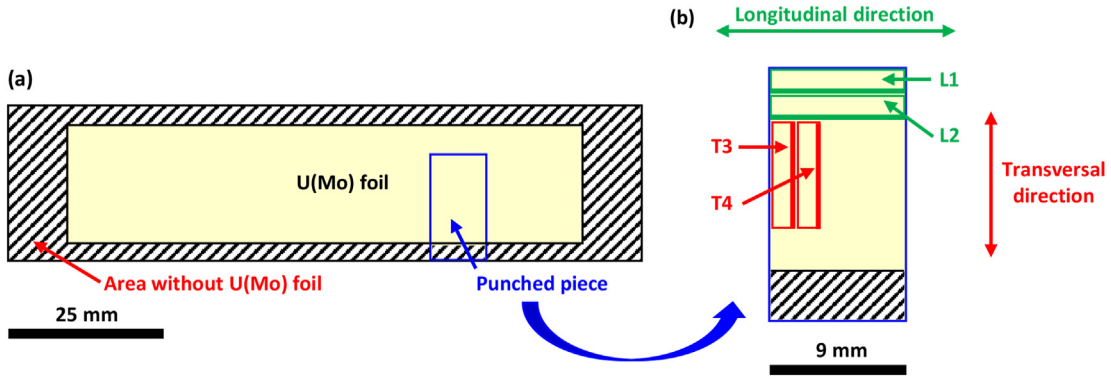

Fig. 1. Cutting plans of (a) the n° 1205 archive mini-plate, (b) the piece punched from this mini-plate.

3. Results and discussion

The results presented in this section are either specific to longitudinal or transversal samples, if specified, or representative of both types of samples, when only one sample is presented. Preliminary macrographic examinations showed that L1 and L2 samples were bent at their ends. Moreover, L1 presented a dozen cracks propagating from its convex side in the U(Mo) foil (see supplementary material). As the T3 sample was practically not bent but exhibited similar cracks and as these two samples were the closest ones to the edges of the original piece, most of the cracks are not a consequence of bending but most likely come from the punching method used to cut a piece from the original mini-plate at Framatome-CERCA.

To make the text more fluid and easier to follow, it was chosen to discuss the results obtained as they are presented.

3.1. OM and SEM + EDS examinations

Fig. 2 gathers three representative micrographs taken at different magnifications on L1 and T3 samples. The grains in the U(Mo) foil are visible thanks to a thin superficial oxidation that occurs after keeping the sample at least one day in air after polishing. This oxidation varies with the grain crystallographic orientation and leads to small color changes. The size of the grains is several tens of micrometers wide and up to one hundred micrometers long, their shape being clearly elongated in both samples (see in particular Fig. 2b). There is no visible sign of destabilization of the γ-U(Mo) phase into α-U, as no lamellar or cellular regions are observed, contrary to the results of observations performed on other monolithic fuels: see for example Fig. 1 in Ref. [9], related to a non-optimized monolithic plate.

Many dark precipitates are also visible in the foil (Fig. 2b). They can be divided into two families: (i) sub-micrometric precipitates which are numerous and distributed in wavy veins, (ii) fewer large precipitates of the order of a few to about 10 μm. These large particles are often cracked (Fig. 3a and b). EDS point analyses indicate that the large precipitates are C-rich and thus correspond to uranium carbides (UC), as illustrated qualitatively by Fig. 3c. The small ones cannot be analyzed by EDS in the SEM, since their size is smaller than that of the X-ray emission volume and since carbon is present on the whole sample surface as a contaminant. However, as their contrast in BackScattered Electron (BSE) mode is the same as that of the large ones (Fig. 3a), they are also most probably carbides. The presence of carbides in monolithic U(Mo) alloys has been reported by many authors (see for example [6,9,17–19]). Hot rolling reduction passes lead to their redistribution to form stringers and cold rolling induces the fracturing of the large ones [19]. Some oxide, silicide or other complex particles were also observed in some studies [9,18,20,21], but were not encountered in this foil. This does not mean that such particles are definitively absent, since precipitates were not deeply characterized in this work.

The Zr coating has a fairly constant thickness of about 15 μm. In the longitudinal samples (L1 and L2), it presents relatively wide cracks partly filled by Al, as illustrated by Fig. 2a and c (the latter corresponding to the area framed in yellow in Fig. 2a) and also by Fig. 4a taken by SEM in BSE mode. This particularity would be linked to the foil biasing during the coating which leads to a high coating hardness (of the order of 300 HV), according to the TUM experience and literature ([22] for example). Indeed, biasing controls the bombardment of the sample surface by ions and thus affects different properties of the coating such as its stress state and microstructure. In the present case, biasing tends to favor the coating fracture during the rolling process, the wider cracks being then filled with aluminium. Such large cracks are not encountered in the transversal samples (T3 and T4). Thinner cracks cross the Zr layer in L1 and T3 samples, and sometimes propagate in the U(Mo) foil over distances up to 100 μm, or even more (Fig. 2a). As previously discussed, these thin cracks probably come from the punching of the piece from the plate.

The micrograph presented in Fig. 4b (taken in Secondary Electron (SE) mode) was taken in a locally broken part of the coating (this breakage having occurred during polishing). It reveals columnar grains within the coating, the largest ones reaching a diameter of about 1 μm, and a length of a few micrometers. This observation is consistent with that presented in Fig. 2c, taken in a non-broken part of the layer, where columnar grains were also discernible. Such a grain-morphology is often observed in PVD coatings [23]. It depends on deposition parameters which influence the nucleation and growth mechanisms of the film [24].

At this observation scale and with these conditions of contrast, the cohesion of the cladding onto Zr coating and Zr onto U(Mo) foil seem to be good, but some decohesions were observed locally mainly at the cladding/Zr interface, some of them spreading over a

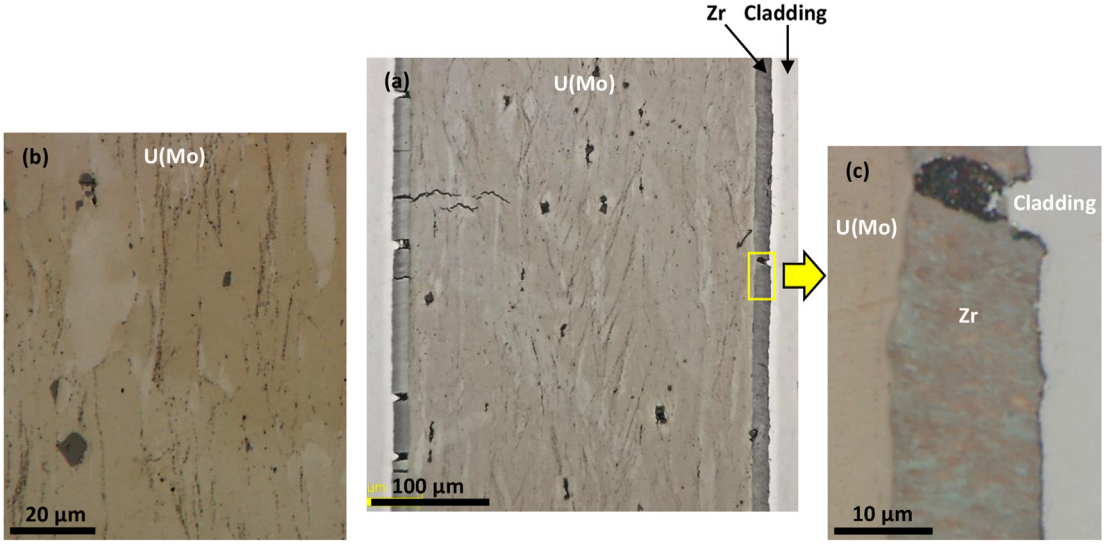

Fig. 2. Optical micrographs taken at different magnifications on samples L1 (for (a) and (c)) and T3 (for (b)).

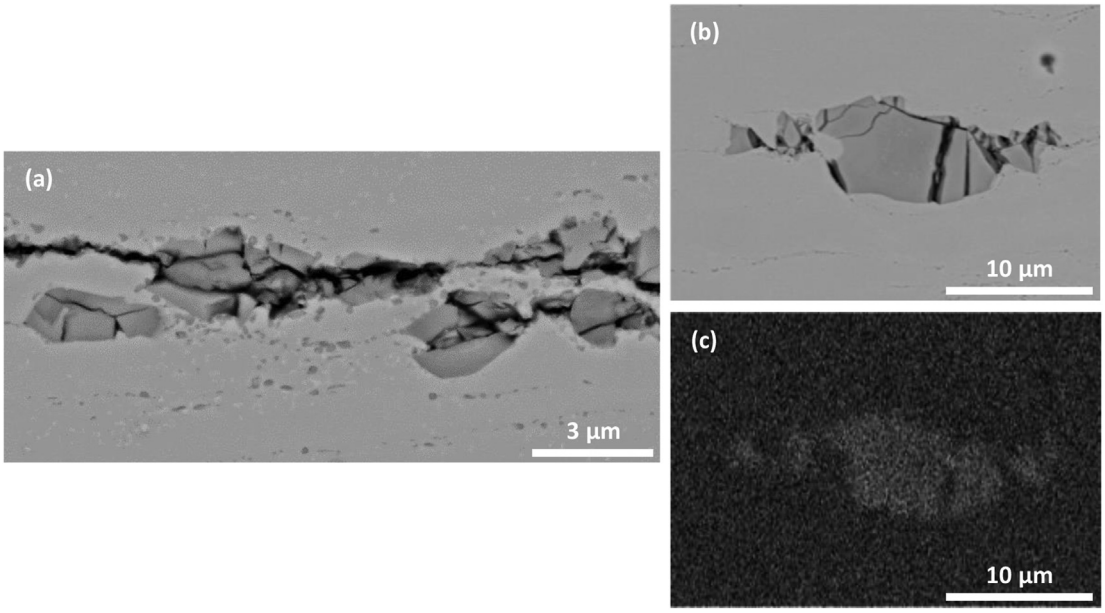

Fig. 3. SEM observation (BSE mode) of precipitates in samples T3 (a) and L1 (b), (c) C-Kα X-ray map acquired by EDS on the area corresponding to (b).

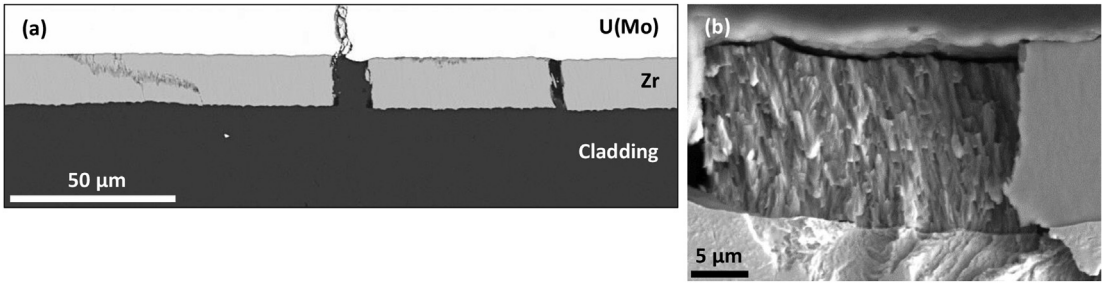

Fig. 4. SEM micrographs taken close to the interface between the fuel and the cladding in the sample L1, (a) in BSE mode (b) in SE mode, in an area where the coating is locally broken.

hundred micrometers or more, as illustrated by Fig. 5 (white arrows). These decohesions could be due to the punching of the piece and/or the mechanical polishing of the samples. It is worth noting that such decohesions were mostly encountered in transversal samples.

Line-scans were performed by EDS on samples L1 and T3, to evaluate the Mo distribution homogeneity. They led to a 10.3 wt% mean Mo content, with fluctuations of the order of ±0.5 wt%. These fluctuations can be reasonably attributed to the inherent dispersion of EDS analyses (i.e. ± 5% relative to the correct value [25]). The values obtained for standard deviations are close to those given by Clarke et al. for Electron Probe MicroAnalysis (EPMA) results collected on U(Mo) samples homogenized at 1273 K [26]. They are also close to those measured by EDS, in UO_2 Laboratory (CEA Cadarache), on homogenized atomized particles (unpublished results). This suggests that the U(Mo) alloy used to manufacture the foil was homogenized at high temperature before rolling, as usually done at BWXT [27].

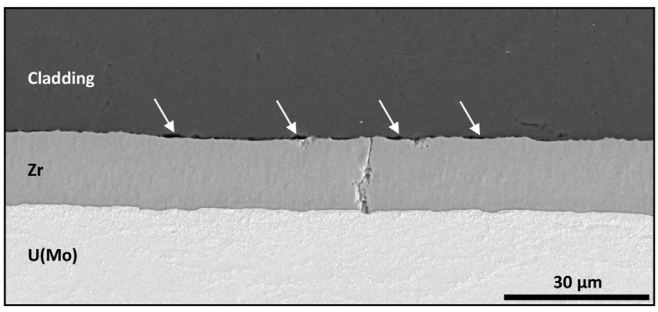

Fig. 5. SEM micrograph (SE mode) taken in the sample T3 (transversal direction) in an area where decohesions are present at the cladding/Zr interface (white arrows).

Complementary examinations were performed by SEM at relatively high magnifications in order to try to evidence the potential presence of interaction layers at cladding/Zr and Zr/U(Mo) interfaces. The four samples were observed on their both sides. Fig. 6 shows typical micrographs. At the cladding/Zr interface, an almost continuous medium grey layer is visible (Fig. 6a). Since it is 100–300 nm thick, its elemental composition cannot be analyzed accurately by EDS in the SEM, to check if it could correspond to an Al/Zr interdiffusion zone formed during the manufacturing of the mini-plate. At the Zr/U(Mo) interface, a very thin (≤100 nm) and discontinuous layer is observed (Fig. 6b), and cannot be analyzed either.

TEM examinations, coupled with EDS analyses of FIB lamellas, i.e. with a high spatial resolution, are essential to determine the nature of the layers observed at both interfaces.

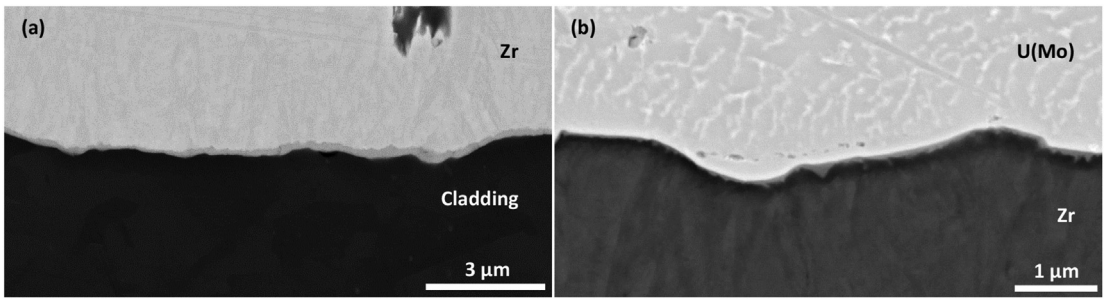

Fig. 6. SEM micrographs in BSE mode of (a) cladding/Zr interface, (b) Zr/U(Mo) interface (sample T3).

3.2. EBSD

Several authors published EBSD characterizations performed on U(Mo) alloys at different steps of the monolithic fuel manufacturing process [26,28,29]. In these studies, samples were prepared either by electropolishing, or by mechanical polishing. However, to our best knowledge, the microstructure of the Zr layer has never been analyzed by EBSD, whatever the type of coating method. Likewise, only few EBSD results seem to have been published about the cladding (see for example [6]).

As indicated in section 2.1., two polishing methods were used in this work: a mechanical one, making the study of the U(Mo) foil and of the cladding possible and FIB milling for providing useable EBSD data for Al, Zr and U(Mo) at the same time. Fig. 7 and Fig. 8 illustrate results after mechanical polishing obtained in the cladding close to its interface with Zr and in the middle part of the U(Mo) foil, respectively.

In the cladding, the EBSD map was acquired with a 0.16 µm step size and with a 2 × 2 pixel camera binning. The raw indexation rate was a bit low before noise reduction (75%, excluding the non-indexed Zr layer from the data), since polishing defects and precipitates were not indexed. A standard cleaning of the data allowed reaching an indexation rate of 86%. Fig. 7b presents the EBSD map obtained after this process. Grain boundaries, with misorientations greater than 10° are drawn as black lines on this map and non-indexed areas (e.g. polishing defects, precipitates) are also displayed in black. In the cladding, grains are relatively small and are often elongated perpendicular to the cladding/Zr interface. Their mean size, in equivalent circular diameter (ECD), is about 1.3 µm (excluding grains with an area lower than 10 pixels, as recommended by ISO 13067 standard [30]). This value is a little rough, since the step size used to acquire this map (0.16 µm) is a bit large compared to the grain size [30].

The U(Mo) foil was analyzed by EBSD, close to its interface with the Zr coating and in its central part. Similar characteristics were found in these different areas. They are illustrated by Fig. 8, which corresponds to a map acquired in the central part of the foil, with no camera binning. In these conditions, a very good indexation rate was achieved: 96% for raw data, and 99% for cleaned ones. Almost the whole area was indexed as corresponding to γ-U(Mo) phase, except some polishing defects and small carbides (in black). This result confirms that no significant destabilization of this phase occurred during the plate manufacturing process. In Fig. 8a, grain boundaries corresponding to misorientations greater than 10° are drawn in black. They delimite large elongated grains, as expected from OM examinations (Fig. 2). These grains present gradual color variations which reflect progressive orientation gradients. It is also illustrated by Fig. 8b which shows a misorientation profile along a black line drawn in Fig. 8a and reveals orientation variations of several degrees within the grain. Such microstructural features tend to indicate that, at the end of the whole manufacturing process of the plate, the U(Mo) foil did not undergo complete recovery, leading to sub-grains with well-defined low misorientation boundaries, or recrystallization, leading to new equiaxed grains [31]. A similar microstructural state was observed by Frazer et al. in a full-length monolithic plate (manufactured within the AFIP-7 irradiation campaign [32]) and was interpreted as reflecting the presence of dislocation pile-up within grains [33]. For comparison, recrystallized microstructures obtained after post-rolling heat treatments can be found in Refs. [28,29,34], for example. It is not possible to go further in the discussion concerning the microstructure of the U(Mo) foil, compared to that observed by other

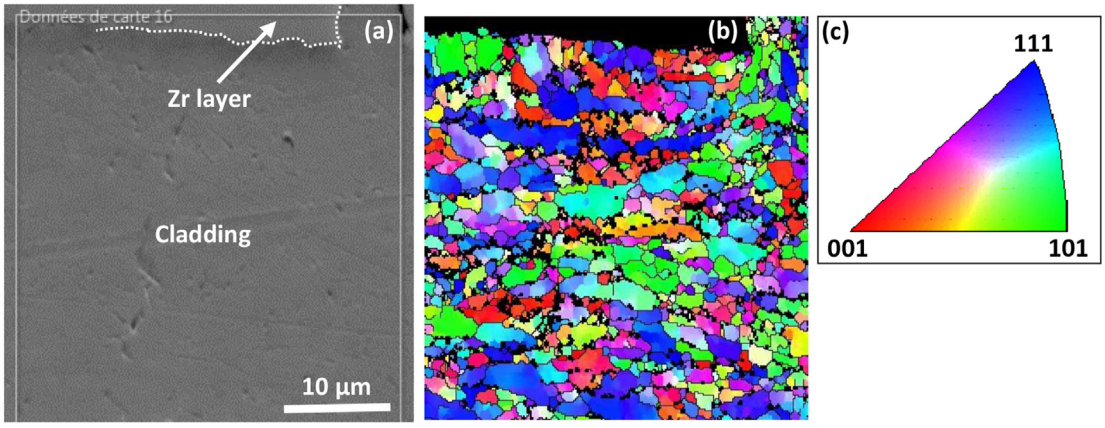

Fig. 7. EBSD analysis of the cladding close to the Zr layer in sample L1, (a) SEM micrograph in SE mode, (b) EBSD map with Al grains colored according to the IPF-Z color code given in (c). Grain boundaries with misorientation greater than 10° are drawn as black lines and non-indexed points are also displayed in black.

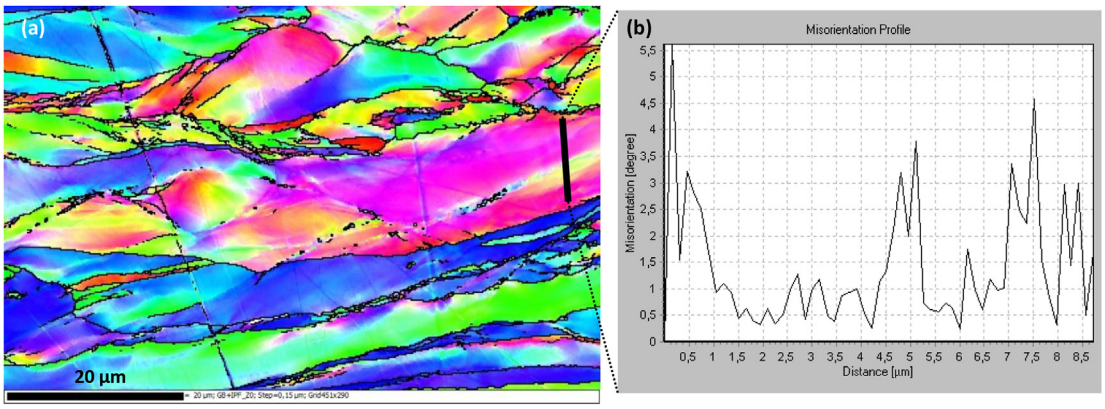

Fig. 8. EBSD analysis of the U(Mo) foil in sample L1, (a) EBSD map with U(Mo) grains colored according to the IPF-Z color code given in Fig. 7c, (b) misorientation profile along the line drawn in black in (a) (from top to bottom).

authors, because details about the C2TWP process are not available (protected by Framatome).

FIB milling was implemented to try to obtain simultaneously good EBSPs in the Al alloy, in Zr and in U(Mo). This polishing method is only applicable on relatively small areas (of a few tens of micrometers). First milling tests were performed using conditions close to those used on U(Mo) atomized particles [15], i.e. with an angle of incidence of the ion beam of a few degrees, relative to the sample surface. Two main issues were identified: (i) the re-deposition of sputtered material behind the abrasion front that damages the quality of EBSPs, (ii) the difficulty to obtain simultaneously satisfactory EBSPs in the cladding, in Zr and in U(Mo). By increasing this angle up to 30°, it was possible to analyse grains correctly in the three studied zones, as illustrated by Fig. 9.

The map presented in Fig. 9 was acquired with a small step size (0.05 µm), chosen in accordance with the expected sub-micrometric grain size in the Zr layer, and no camera binning. An indexation rate of 74% was achieved for this map and reached about 80%, after a moderate cleaning of EBSD data. Grains found in the cladding and in the U(Mo) foil are similar to those respectively shown in Figs. 7 and 8, in terms of size and shape, even if they seem a little more elongated in the cladding. This slight difference is probably due to local microstructural variations and/or distortion effects linked to small drifts during the acquisition.

Furthermore, in the Zr layer, grains were sufficiently numerous to evaluate their size, with a good statistic and a mean grain size of 0.3 µm (in equivalent circular diameter) was determined. Actually, as shown by Fig. 9c, grains are smaller close to the U(Mo) side of the layer and larger with a more marked columnar morphology, close to the Al side. Some of them can reach a length of a few micrometers, in accordance with SEM examinations presented in Fig. 4c. It is common to observe a grain size gradient in PVD coatings, because grain growth becomes easier than nucleation as deposition proceeds [35].

3.3. Preparation of TEM lamellas by FIB

Sample T4 was selected to evaluate the feasibility of preparing TEM lamellas by FIB at cladding/Zr and Zr/U(Mo) interfaces. The *in situ* lift-out technique was used [36]. Because of differences in ion sputtering rates between Al and Zr on the one hand, and Zr and U(Mo) on the other hand, it was difficult to obtain a regular thinning of each whole lamella. This issue is illustrated by Fig. 10 for both interfaces. Despite these difficulties, it was possible to examine the cladding/Zr and Zr/U(Mo) interfaces, in TEM and STEM modes, and to perform EDS analyses across these interfaces.

3.4. TEM and STEM + EDS

3.4.1. Cladding/Zr interface

Fig. 11 summarizes the main observations carried out using TEM and STEM + EDS on the cladding/Zr lamella, and particularly on the interface between these two materials. Figs. 11a and b provide general views of the lamella taken in TEM bright field (BF) and in

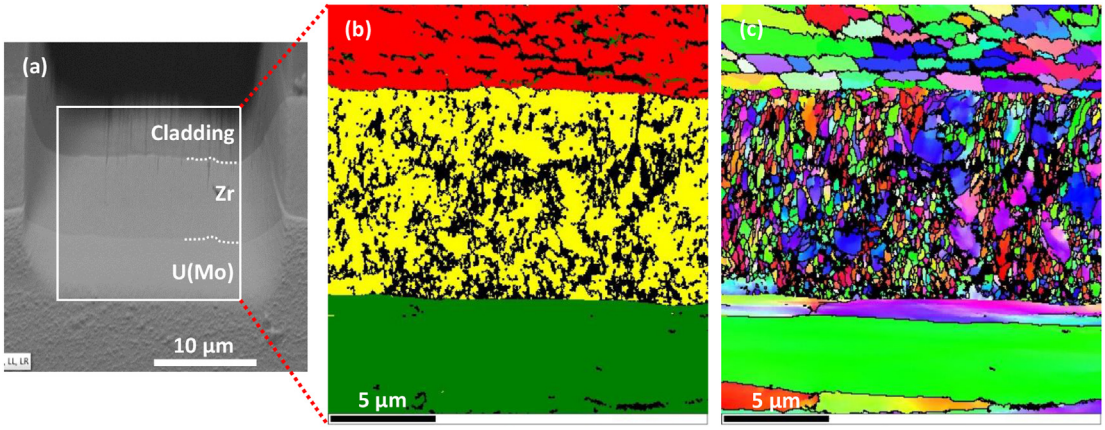

Fig. 9. EBSD analysis of sample T4 after FIB milling with a 30° incidence angle of ion beam, (a) SEM image of the ion milled area, (b) EBSD map colored by phases with Al in red, Zr in yellow and U(Mo) in green, (c) EBSD map in IPF-Z. Grain boundaries with misorientations greater than 10° are drawn in black and non-indexed points are also displayed in black.

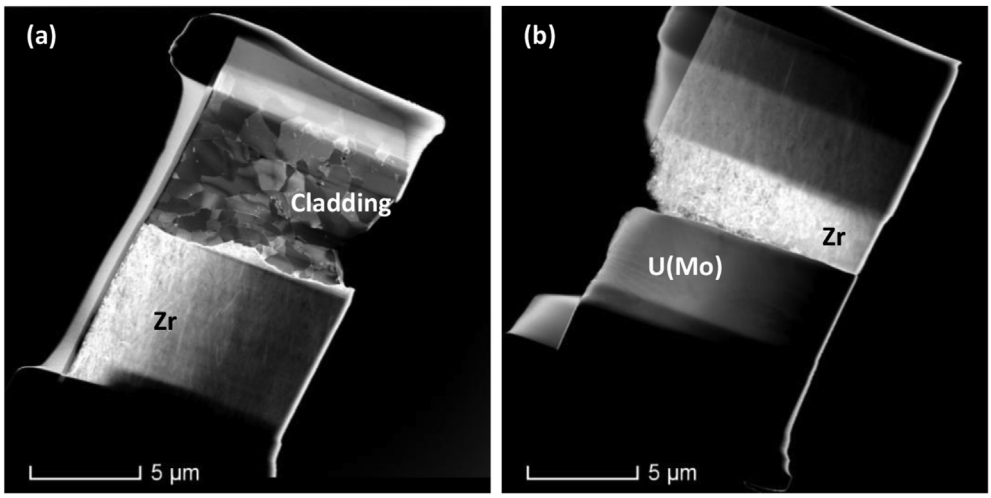

Fig. 10. STEM images in High Angle Annular Dark Field (HAADF) mode of the lamellas located at (a) the cladding/Zr and (b) the Zr/U(Mo) interfaces.

STEM High Angle Annular Dark Field (HAADF) modes, respectively. As previously discussed, the Zr layer appears significantly thicker than the Al-based part. The Zr coating appears fully dense, with no micro-cracks or pores. Columnar grains are observed in it, in accordance with previous examinations. Their diameter is typically of the order of a few hundred nanometers and their length can reach several micrometers. A thin dense intermediate layer (about 100–150 nm thick) is present at the cladding/Zr interface. A part of it is bounded by red dotted lines in Fig. 11a and b. This layer most probably corresponds to that observed by SEM (Fig. 6a). To determine its nature, EDS analyses were performed through the cladding/Zr interface. Fig. 11c shows the Al, O and Zr composition profiles acquired along the yellow arrow drawn in Fig. 11b. It shows that the intermediate layer is almost Al-free, with no substantial concentration gradient typical for an interdiffusion layer. It probably corresponds to an oxidized part of the Zr coating, with an O/Zr + O atomic ratio close to 2/3, i.e. close to that of ZrO_2.

According to examinations performed at higher magnification on the area boxed in green in Fig. 11b, this oxidized layer is nanocrystallized, as shown by Fig. 11d where grains of about a few tens of nanometers are visible. A Selected Area Electron Diffraction (SAED) pattern obtained in this area is presented in Fig. 11e (left hand side). Incomplete rings with dots, typical of the simultaneous diffraction of several grains, are present. The diameter of the first rings is compared to those characterizing monoclinic zirconia (α-ZrO_2), drawn in the right-hand side of Fig. 11e. Even if distances cannot be determined with a high accuracy on these very partial rings, all of them can be attributed to this oxide phase. It is worth noting that the (100) diffraction spots, corresponding to a d_{hkl} of 0.508 nm (cf. grey dotted half circle, in Fig. 11e) are missing in the experimental diffraction pattern. In fact, these spots are masked by the beam stop, but have been observed on other diffraction patterns acquired without this stop (not presented, because they are overexposed).

On the basis of these different results, it can be concluded that the layer present at the interface between the cladding and the Zr coating is not an Al–Zr interdiffusion layer but corresponds to a zirconia layer. This oxide layer does not seem to damage the fuel-cladding cohesion, at least at the scale of the lamella. It probably formed on the Zr coating during the shipment and/or storage of the coated U(Mo) foil, before it was clad with Al.

According to several authors, monolithic plates cladded by Hot Isostatic Pressing (HIP) present Al–Zr interactions layers of micrometric thickness [6,7,37,38]. This manufacturing process involves a relatively long holding time at high temperature (833 K for 90 min, according to Ref. [6], for example) which allows the formation of such layers. According to the present observations, the C2TWP process does not promote any Al–Zr interaction. In addition, the zirconia layer covering the Zr coating could play a certain barrier role against Al–Zr interdiffusion. Excluding cracks observed in the coating in longitudinal samples, and other thinner and longer ones propagating in the foil due to cutting and polishing of samples, no defects were observed in this layer whatever the examination scale, while various defects were observed in electro-plated and plasma-sprayed Zr layers and also in a lower amount in co-rolled ones [8]. However, the question of decohesions observed locally by SEM mainly at the cladding/Zr interface should be clarified: are they a consequence of sample preparation or not? Non-destructive methods such as ultrasonic testing were developed to characterize as-manufactured fuel plates [39] but their results are relatively difficult to interpret at this point.

3.4.2. Zr/U(Mo) interface

The results of the TEM examinations of the Zr/U(Mo) interface are summarized in Fig. 12. The first image (Fig. 12a), taken at relatively low magnification, shows that even if the U(Mo) part of the lamella is thicker than the Zr one (as already shown in Fig. 10b), it is exploitable for TEM examinations. No thin layer is present at the Zr/U(Mo) interface. This result indicates that the final thinning of the lamella took place in a layer-free zone as, at the SEM scale, only a very thin and discontinuous layer was observed (Fig. 6b).

The image presented in Fig. 12b was taken in the Zr layer, close to its interface with U(Mo). It reveals a complex microstructure, with columnar grains smaller than those encountered close to the cladding (Fig. 11a and b), in accordance with EBSD results (Fig. 9c). Like near the cladding/Zr interface, the coating appears fully dense, with no visible defects such as cracks or voids. Structural defects, such as dislocations, were not examined in detail but are probably present.

Figs. 12c and d presents TEM images acquired in the same area of the U(Mo) foil, with two different α-tilt conditions. Bend contours and numerous small dark dots are visible in Fig. 12c. According to the laboratory feedback, these dots probably correspond to small dislocation loops induced by FIB milling, as observed by many authors on different materials (see for example [40]). To check it, very gentle ion milling should be performed at low energy after FIB milling in order to eliminate these defects. Thanks to tilt conditions leading to their extinction, these dots are almost invisible in

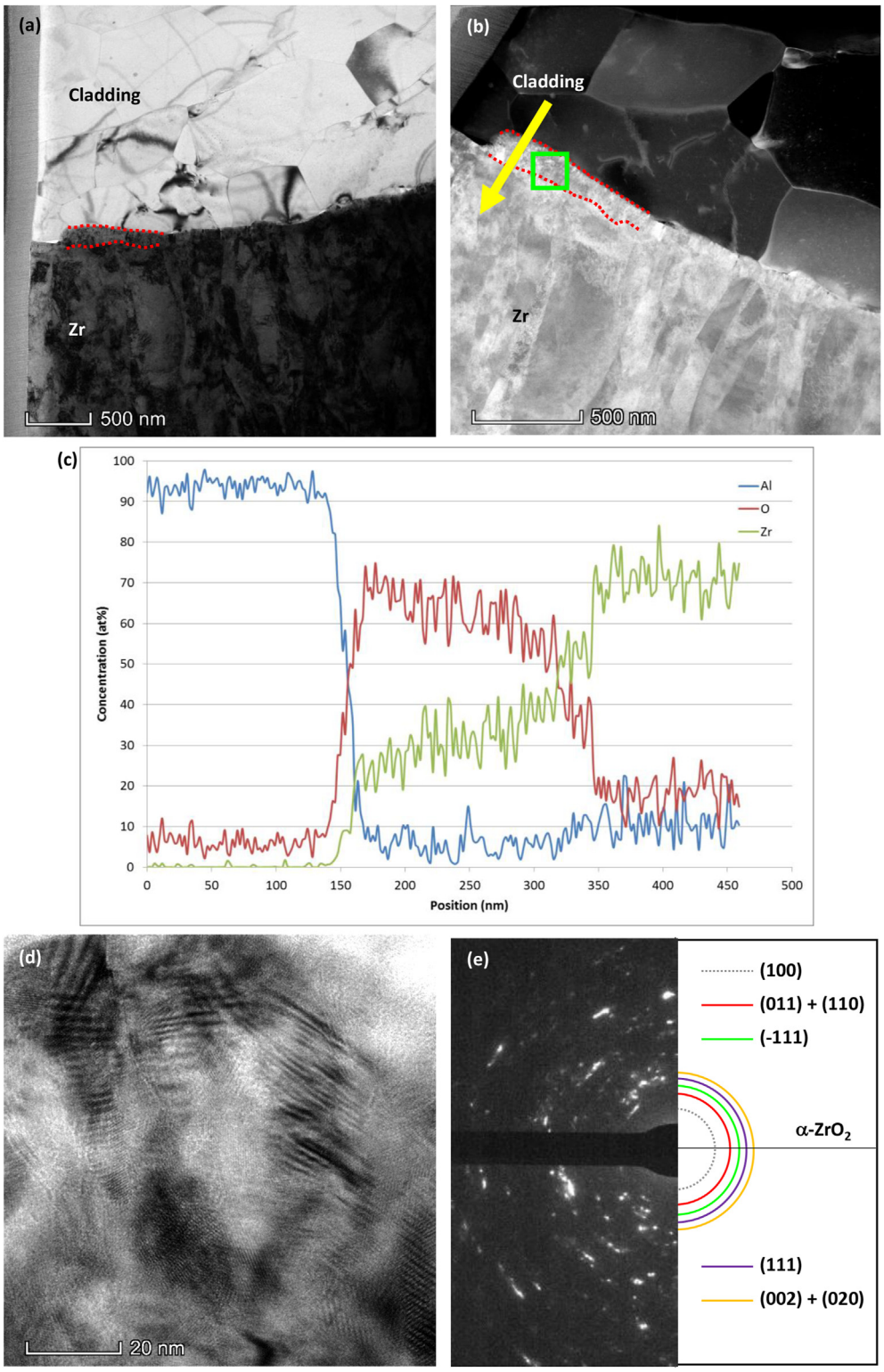

Fig. 11. Cladding/Zr lamella observed (a) by TEM (BF mode), (b) by STEM (HAADF mode), (c) Al, O and Zr composition profiles measured by EDS along the yellow arrow drawn on image (b), (d) interfacial layer observed by TEM at high magnification (BF mode), (e) SAED pattern of the interfacial layer shown in (d) compared to the theoretical diffraction pattern of polycrystalline α-ZrO_2 (for the first diffracting planes).

Fig. 12d, where relatively long tangled dislocations arranged in irregular lines (pointed by several white arrows) are now clearly visible. The presence of these dislocations is consistent with EBSD results, which highlighted the existence of orientation gradients within the grains (Fig. 8). They do not form well-defined networks (i.e. sub-boundaries), which tends to confirm that at the end of the manufacturing process (for which details are not available) no complete recovery occurred within the U(Mo) grains. These

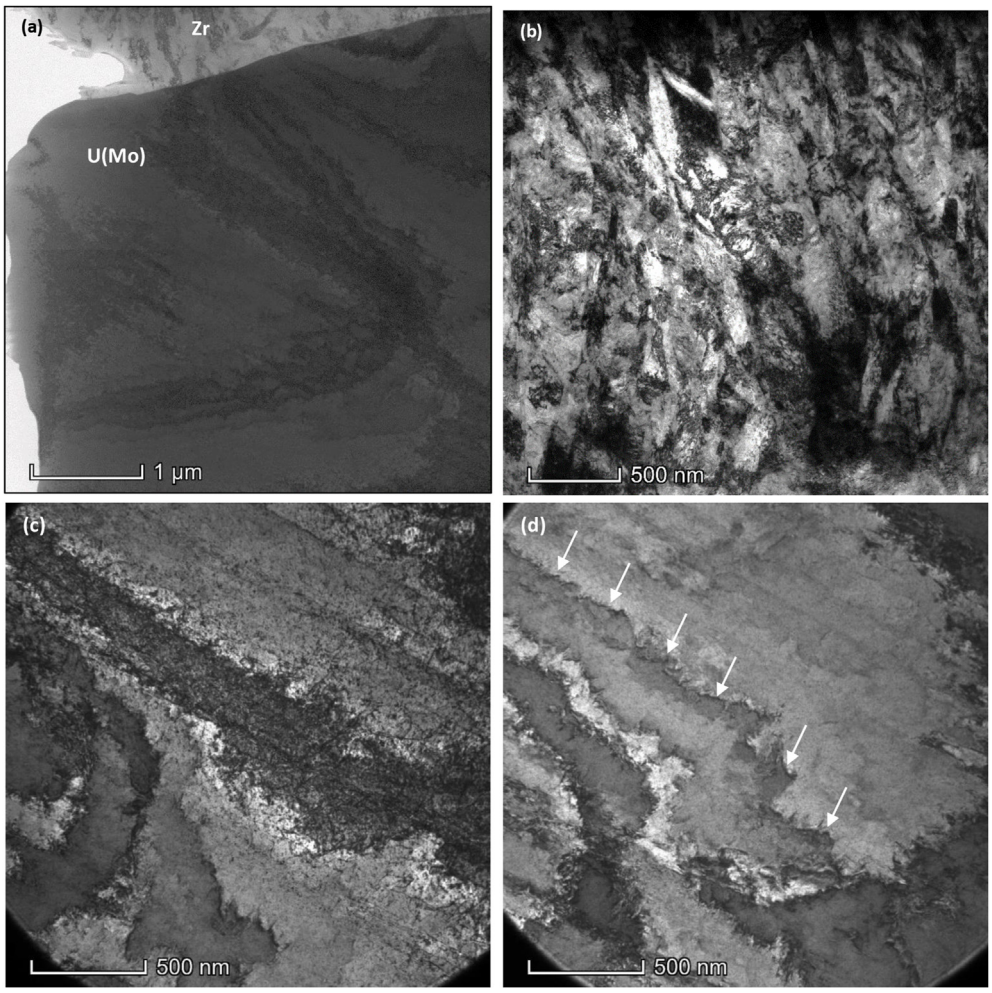

Fig. 12. TEM observations of Zr/U(Mo) lamella (BF mode), (a) Zr/U(Mo) interface, (b) Zr layer, (c) U(Mo) (α-tilt: 10°), (d) same area in U(Mo) (α-tilt: 15°).

observations are also fully consistent with the dislocation pile-up within grains mentioned by Frazer et al., on the basis of EBSD results obtained on a full-size monolithic plate [33]. No signs of decomposition of the γ-U(Mo) phase into α-U were found at TEM scale, whereas such destabilization were observed by TEM on plates cladded by HIP near the eutectoid temperature [41]. However, it would be necessary to observe larger areas in γ-U(Mo) including grain boundaries, to be definitively sure that no decomposition started to occur (even if examinations by OM and SEM did not evidence any signs of that process).

EDS analyses performed at the Zr/U(Mo) interface confirmed that no intermediate layer was present at the Zr/U(Mo), in this lamella. Studies performed on HIP bonded plates showed that micrometer thick interaction layers can develop at this interface [6,8,9]. According to the present work, the C2TWP process does not promote such interactions. The very thin layer hardly observed by SEM at the Zr/U(Mo) interface (Fig. 6b) could correspond to a thin oxide film formed on the U(Mo) foil as a consequence of its rolling, etching and/or storage conditions before its coating [42]. It could perhaps also correspond to a very thin and local interaction layer between U(Mo) and Zr. Taking into account the small size of FIB lamellas and the scarcity of this tiny layer, it would be difficult to check these assumptions, by preparing and observing other lamellas. In any case, no consequence on the U(Mo)/Zr cohesion has been evidenced.

4. Conclusions

The EMPIrE irradiation experiment performed in the ATR comprised four U(Mo) monolithic fuel mini-plates. In two of them, the monolithic U(Mo) foil provided by BWXT had been PVD-coated with Zr at FRM II (TUM, Germany), before the plate manufacturing by Framatome-CERCA (France). This study is the first one performed on a Zr-PVD coated U(Mo) monolithic fresh fuel mini-plate. Four samples were studied: two longitudinal and two transversal ones.

Main results related to the U(Mo) foil are as follows: microstructural examinations showed that the grains had a size of several tens of micrometers and an elongated shape. No signs of γ-U(Mo) destabilization were noticed in the whole foil, but larger areas should be examined at TEM scale to confirm this point. As frequently observed in monolithic plates, many carbides were present in the foil: a large part of them were small (micrometric) and formed veins, approximately aligned with the long axis of the U(Mo) grains, some were larger (several micrometers) and more scattered. According to Mo composition profiles, the U(Mo) alloy was homogenized at high temperature. EBSD maps revealed orientation gradients within the U(Mo) grains and TEM examinations revealed the presence of numerous tangled dislocations in these grains, which were not organized in well-defined networks. These results tend to indicate that, at the end of the manufacturing process, neither complete recovery nor recrystallization occurred

within the U(Mo) grains. Modifying this process in order to reduce the density of defects present in the foil could favor a better behavior of the fuel under irradiation, by delaying recrystallization due to the accumulation of irradiation defects in the U(Mo) grains and reducing the resulting fuel swelling.

The Zr coating has a thickness around 15 μm. This coating has a columnar microstructure, with grains with a diameter in the range of a few hundred nanometers and a length varying from one to several micrometers, the largest grains being encountered close to the cladding/Zr interface. Excluding large cracks probably partly due to cutting and polishing of samples, no micro-cracks or pores were encountered in this layer, whatever the examination scale. The cohesion of the cladding/Zr and Zr/U(Mo) interfaces seems to be good, even if decohesions were observed locally mainly at the cladding/Zr interface in transversal samples, perhaps due to polishing operations.

A particular attention was paid to the examination of the cladding/Zr and Zr/U(Mo) interfaces, to find eventual interdiffusion layers, similar to those encountered in monolithic plates cladded by HIP. According to SEM, at the cladding/Zr interface, an almost continuous layer with a thickness of about 100–300 nm is present, while at the Zr/U(Mo) interface, a very thin ($\leq$100 nm) and discontinuous layer is observed. STEM + EDS observations, carried out on lamellas prepared by FIB, showed that the layer present at the cladding/Zr interface corresponded to an oxidized part of the Zr layer (zirconia), while no intermediate layer was observed at the Zr/U(Mo) interface. The latter small discontinuous layer observed by SEM at the Zr/U(Mo) side could correspond either to locally oxidized U(Mo) or to an interaction layer but could not be analyzed here.

This work provides a basis for interpreting the results of characterizations planed on EMPIrE irradiated plates.

Declaration of competing interest

The authors declare that they have no known competing financial interests or personal relationships that could have appeared to influence the work reported in this paper.

Acknowledgements

This work was supported by the European Commission in the framework of HORIZON 2020 through Grant Agreement 754378 in the LEU-FOREvER project and preparatory work at TUM was supported by a combined grant (FRM1318) from the Bundesministerium für Bildung und Forschung and the Bayerisches Staatsministerium für Bildung und Kultus, Wissenschaft und Kunst.

Appendix A. Supplementary data

Supplementary data to this article can be found online at https://doi.org/10.1016/j.net.2021.02.026.

References

[1] Y.S. Kim, Uranium intermetallic fuels (U-Al, U-Si, U-Mo), Comprehensive Nuclear Materials 3 (14) (2012) 392–422.
[2] Safety evaluation report related to the evaluation of Low Enriched Uranium silicide-aluminum dispersion fuel for use in non-power reactors, U.S. Nuclear Regulatory Commission (1988). NUREG-1313.
[3] S. Van Den Berghe, P. Lemoine, Review of 15 years of high-density, low enriched UMo dispersion fuel development for research reactors in Europe, Nucl. Eng. Technol. 46 (2014) 125–146.
[4] M.K. Meyer, J. Gan, J.F. Jue, D.D. Keiser, E. Perez, A. Robinson, D.M. Wachs, N. Woolstenhulme, G.L. Hofman, Y.S. Kim, Irradiation performance of U-Mo monolithic fuel, Nucl. Eng. Technol. 46 (2014) 169–182.
[5] G.A. Moore, M.C. Marshall, Co-rolled U10Mo/Zirconium-Barrier-Layer Monolithic Fuel Foil Fabrication Process, Idaho National Laboratory, 2010. INL-EXT-10-17774.
[6] J.F. Jue, D.D. Keiser, C.R. Breckenridge, G.A. Moore, M.K. Meyer, Microstructural characteristics of HIP-bonded monolithic nuclear fuels with a diffusion barrier, J. Nucl. Mater. 448 (2014) 250–258.
[7] R. Newell, A. Mehta, Y.J. Park, D.D. Keiser, Y.H. Sohn, Interdiffusion, reactions and phase transformations observed during fabrication of low enriched uranium monolithic fuel system for research and test reactors, Defect Diffusion Forum 383 (2018) 10–16.
[8] R. Newell, A. Mehta, Y.J. Park, D.D. Keiser, J.J. Cole, Y.H. Sohn, Microstructural characteristics of plasma sprayed, electroplated, and co-rolled Zr diffusion barriers in hot isostatic pressed low enriched U-10 wt% Mo monolithic fuel plates, J. Nucl. Mater. 523 (2019) 91–100.
[9] D.D. Keiser, J.F. Jue, B. Miller, J. Gan, A. Robinson, J. Madden, Observed changes in as-fabricated U-10Mo monolithic fuel microstructures after irradiation in the Advanced Test Reactor, J. Occup. Med. 69 (2017) 2538–2545.
[10] J.F. Jue, D.D. Keiser, B.D. Miller, J.W. Madden, A.B. Robinson, B.H. Rabin, Effects of irradiation on the interface between U-Mo and zirconium diffusion barrier, J. Nucl. Mater. 499 (2018) 567–581.
[11] I. Glagolenko, G. Housley, A. Robinson, M. Bybee, M. Hammond, J. Nielsen, D. Crawford, J. Wiest, J. Jacobson, The European Miniplate Irradiation Experiment (EMPIrE), RRFM, Jordan, 2019. March 24-28.
[12] C. Steyer, B. Baumeister, C. Schwartz, W. McCollough, C. Reiter, F. Alder, T. Dirks, D. Bach, T. Huber, H. Breitkreutz, W. Petry, B. Stepnik, M. Grasse, C. Moyroud, R. Johnson, R. Mayfield, G. Argon, Production of Monolithic UMo Plates for the EMPIrE Irradiation Experiment, RERTR, Antwerp, Belgium, 2016. October 23-27.
[13] B. Stepnik, M. Grasse, C. Jarousse, D. Geslin, J. Schulthess, I. Glagolenko, A. Yacout, S. Bhattacharya, T. Wiencek, M. Pellin, S. Van Den Berghe, A. Leenaers, H. Breitkreutz, T.K. Huber, T. Zweifel, W. Petry, M. Delpech, H. Palancher, Y. Calzavara, H. Guyon, Manufacturing Progress Status of EMPIrE UMo Irradiation Experiment, RERTR, Antwerp, Belgium, 2016. October 23-27.
[14] I. Glagolenko, N. Woolstenhulme, M. Lillo, J. Nielsen, D. Choe, J. Navarro, C. Jensen, D. Crawford, W. Jones, S. Snow, B. Hawkes, J. Wiest, D. Keiser, K. Holdaway, J. Schulthess, B. Rabin, Status Update on Mini-Plate Experiment Designs Planned for Irradiation in the Advanced Test Reactor, RRFM, Berlin, Germany, 2016. March 13-17.
[15] X. Iltis, I. Zacharie-Aubrun, H.J. Ryu, J.M. Park, A. Leenaers, A.M. Yacout, D.D. Keiser, F. Vanni, B. Stepnik, T. Blay, N. Tarisien, C. Tanguy, H. Palancher, Microstructure of as-atomized and annealed U-Mo7 particles: a SEM/EBSD study of grain growth, J. Nucl. Mater. 495 (2017) 249–266.
[16] K. Thomsen, N.H. Schmidt, A. Bewick, K. Larsen, Improving the accuracy of orientation measurements using EBSD, Microsc. Microanal. 19 (2013) 724–725.
[17] E.A. Nyberg, D.E. Burkes, V.V. Joshi, C.A. Lavender, The Microstructure of Rolled Plates from Cast Billets of U-10Mo Alloys, Pacific Northwest National Laboratory, 2015. PNNL-24160.
[18] Y. Park, N. Eriksson, D.D. Keiser, J.F. Jue, B. Rabin, G. Moore, Y.H. Sohn, Microstructural anomalies in hot-isostatic U-10 wt.% Mo fuel plates with Zr diffusion barrier, Mater. Char. 103 (2015) 50–57.
[19] X. Hu, X. Wang, V.V. Joshi, C.A. Lavender, The effect of thermomechanical processing on second phase particle redistribution in U-10 wt% Mo, J. Nucl. Mater. 500 (2018) 270–279.
[20] A. Devaraj, L. Kovarik, E. Kautz, B. Arey, S. Jana, C. Lavender, V. Joshi, Grain boundary engineering to control the discontinuous precipitation in multi-component U10Mo alloy, Acta Mater. 151 (2018) 181–190.
[21] L. Kovarik, A. Devaraj, C. Lavender, V. Joshi, Crystallographic and compositional analysis of impurity phase U_2MoSi_2C in UMo alloys, J. Nucl. Mater. 519 (2019) 287–291.
[22] C.S. Chen, C.P. Liu, C.Y.A. Tsao, H.G. Yang, Study of mechanical properties of PVD ZrN films, deposited under positive and negative substrate bias conditions, Scripta Mater. 51 (2004) 715–719.
[23] D.S. Rickerby, S.J. Bull, Engineering with surface coatings: the role of coating microstructure, Surf. Coating. Technol. 39/40 (1989) 315–328.
[24] A.Z. Moshfegh, PVD growth method: physics and technology, in: Physics and Technology of Thin Films, World Scientific Publishing company, 2004, pp. 28–53.
[25] D.E. Newbury, N.W.M. Ritchie, Is scanning electron microscopy/energy dispersive X-ray spectrometry (SEM/EDS) quantitative? Scanning 35 (2013) 141–168.
[26] A.J. Clarke, K.D. Clarke, R.J. McCabe, C.T. Necker, P.A. Papin, R.D. Field, A.M. Kelly, T.J. Tucker, R.T. Forsyth, P.O. Dickerson, J.C. Foley, H. Swenson, R.M. Aikin, D.E. Dombrowski, Microstructural evolution of a uranium-10 wt.% molybdenum alloy for nuclear reactor fuels, J. Nucl. Mater. 465 (2015) 784–792.
[27] L.R. Hubbard, C. Arendt, D. Dye, C. Clayton, U-10Mo Baseline Fuel Fabrication Process Description, Pacific Northwest National Laboratory, 2017. PNNL-26880.
[28] S. Jana, N. Overman, T. Varga, C. Lavender, V.V. Joshi, Phase transformation kinetics in rolled U-10 wt.% Mo foil: effect of post-rolling heat treatment and prior γ-UMo grain size, J. Nucl. Mater. 496 (2017) 215–226.
[29] W.E. Frazier, S. Hu, N. Overman, R. Prabhakaran, C. Lavender, V.V. Joshi, Recrystallization kinetics of cold-rolled U-10 wt% Mo, J. Nucl. Mater. 513 (2019) 56–61.
[30] Microbeam Analysis – Electron Backscattered Diffraction – Measurement of Average Grain Size, 2011. ISO 13067 international standard.

[31] J.F. Humphreys, Recrystallization and recovery, in: Materials Science and Technology, Wiley-VCH Verlag GmBH & Co KGaA, 2006, pp. 373–398.
[32] N.E. Woolstenhulme, D. Wachs, M. Meyer, Design and testing of prototypic elements containing monolithic fuel, RERTR, Santiago, Chile (2011). October 23-27.
[33] D. Frazer, D. Jadernas, N. Bolender, J. Madden, J. Giglio, P. Hosemann, Elevated temperature microcantilever testing of fresh U-10Mo fuel, J. Nucl. Mater. 526 (2019) 151746.
[34] N.R. Overman, S. Jana, D.P. Field, C. Lavender, V.V. Joshi, An electron backscatter analysis of grain boundary initiated discontinuous precipitation in U-10Mo, J. Nucl. Mater. 529 (2020) 151940.
[35] P.A. Dearnley, Introduction to Surface Engineering, Cambridge University Press, 2017.
[36] M. Schaffer, B. Schaffer, Q. Ramasse, Sample preparation for atomic-resolution STEM at low voltages by FIB, Ultramicroscopy 114 (2012) 62–71.
[37] E. Perez, B. Yao, D.D. Keiser, Y.H. Sohn, Microstructural analysis of as-processed U-10wt.%Mo monolithic fuel plate in AA6061 matrix with Zr diffusion barrier, J. Nucl. Mater. 402 (2010) 8–14.
[38] Y. Park, J. Yoo, K. Huang, D.D. Keiser, J.F. Jue, B. Rabin, G. Moore, Y.H. Sohn, Growth kinetics and microstructural evolution during hot isostatic pressing of U-10 wt% Mo monolithic fuel plate in AA6061 cladding with Zr diffusion barrier, J. Nucl. Mater. 447 (2014) 215–224.
[39] N.E. Woolstenhulme, S.C. Taylor, G.A. Moore, D.M. Sterbenz, Non-destructive Examination of Fuel Plates for the RERTR Fuel Development Experiments, Idaho National Laboratory, 2012. INL/EXT-12-27225.
[40] M. Andrzekczuk, P. Plocinski, W. Zielinski, K.J. Kurzydlowski, TEM characterization of the artefacts induced by FIB in austenitic stainless steel, J. Microsc. 237 (2010) 439–442.
[41] Y. Park, N. Eriksson, R. Newell, D.D. Keiser, Y.H. Sohn, Phase decomposition of γ-U (bcc) in U-10 wt% Mo fuel alloy during hot isostatic pressing of monolithic fuel plate, J. Nucl. Mater. 480 (2016) 271–280.
[42] T.C. Kaspar, C.L. Arendt, D.L. Neal, S.L. Riechers, C. Rutherford, A. Shemer-Kohrn, S.R. Spurgeon, L.E. Sweet, V.V. Joshi, C.A. Lavender, R.W. Shimskey, Characterization of surface layers formed on DU10Mo ingots after processing steps and high humidity exposure, J. Nucl. Mater. 514 (2019) 28–39.